JGR Oceans

RESEARCH ARTICLE

10.1029/2025JC022762

Warming Trend in the Western Indian Ocean Driven by Oceanic Transport

Ligin Joseph[1], Dipanjan Dey[1,2], Nikolaos Skliris[1], Alejandra Sanchez-Franks[3], Robert Marsh[1], Joel Hirschi[3], and Sreevathsa Golla[1,3]

[1]School of Ocean and Earth Science, University of Southampton, Southampton, UK, [2]School of Earth, Ocean and Climate Sciences, Indian Institute of Technology Bhubaneswar, Khordha, Odisha, India, [3]National Oceanography Centre, Southampton, UK

Key Points:

- A significant increasing trend in the upper (300 m) ocean heat content (OHC) in the northwestern Indian Ocean is shown during 2000–2023
- This increase in OHC is driven by oceanic transport and heat accumulation, particularly during the winter monsoon
- A northward shift of the Great Whirl increases downwelling, reducing cooling in a region typically marked by upwelling

Supporting Information:

Supporting Information may be found in the online version of this article.

Correspondence to:

L. Joseph,
lj3n23@soton.ac.uk

Citation:

Joseph, L., Dey, D., Skliris, N., Sanchez-Franks, A., Marsh, R., Hirschi, J., & Golla, S. (2026). Warming trend in the western Indian Ocean driven by oceanic transport. *Journal of Geophysical Research: Oceans*, *131*, e2025JC022762. https://doi.org/10.1029/2025JC022762

Received 17 APR 2025
Accepted 17 DEC 2025

Author Contributions:

Conceptualization: Ligin Joseph, Dipanjan Dey, Nikolaos Skliris, Alejandra Sanchez-Franks, Robert Marsh
Data curation: Ligin Joseph
Formal analysis: Ligin Joseph, Dipanjan Dey, Sreevathsa Golla
Investigation: Ligin Joseph
Methodology: Ligin Joseph, Dipanjan Dey, Nikolaos Skliris, Alejandra Sanchez-Franks, Joel Hirschi
Resources: Ligin Joseph
Software: Ligin Joseph
Supervision: Dipanjan Dey, Nikolaos Skliris, Robert Marsh, Joel Hirschi
Validation: Ligin Joseph, Dipanjan Dey, Nikolaos Skliris

Abstract The ocean has absorbed over 90% of the excess heat trapped in the Earth system due to rising greenhouse gas emissions, with upper layers playing a crucial role. This study finds that 35% of the total ocean heat content (OHC) in the western Indian Ocean is stored within the upper 300 m. From 2000 to 2023, this layer shows a significant warming trend of 0.87 GJ/m^2 over 24 years, making it the only tropical ocean basin with such a persistent rise. In contrast, the net surface heat flux into the ocean shows a declining trend of −15.90 W/m^2 over 24 years, suggesting that direct atmospheric forcing is not the primary driver. Instead, seasonal ocean dynamics explains the observed increase in OHC and surface heat loss. During the winter monsoon, enhanced westward heat transport from the eastern equatorial Indian Ocean, driven by strengthened northeast monsoon currents, leads to heat accumulation in the western Indian Ocean. In the summer monsoon, the Great Whirl, a large anticyclonic eddy, plays a central role. Although northward heat transport associated with the Great Whirl has weakened, the southward transport has declined more sharply, resulting in net heat gain. Additionally, a northward shift in monsoon winds displaces the Great Whirl closer to the Socotra Islands, altering upwelling patterns and further redistributing heat. These findings underscore the dominant role of ocean circulation in driving long-term upper-ocean warming in the western Indian Ocean, contrasting with the expected influence of surface heat fluxes.

Plain Language Summary The ocean plays a major role in regulating Earth's climate by storing most of the excess heat caused by greenhouse gas emissions. This study focuses on the western Indian Ocean, where we found a significant warming of the upper 300 m of the ocean between 2000 and 2023. Surprisingly, this warming occurred even though the amount of heat entering the ocean from the atmosphere has been decreasing. This suggests that changes in ocean currents, rather than just surface heating, are driving the warming. During the winter season, stronger ocean currents push warm water from the eastern Indian Ocean toward the Arabian Sea. In the summer, a large rotating ocean current called the Great Whirl traps heat in the western Arabian Sea. As monsoon winds have shifted northward, the Great Whirl has moved closer to the Socotra Islands, changing the way deep, cold water rises to the surface. These changes in ocean circulation help explain why heat is building up in this region. Understanding how and why the ocean stores heat is important for predicting future changes in climate, weather patterns, and marine ecosystems.

1. Introduction

The Indian Ocean covers 20% of the world's oceans. It is the only ocean to be landlocked from the north. The northern Indian Ocean is divided into two parts by the Indian subcontinent: the Arabian Sea on the west and the Bay of Bengal on the east. The Bay of Bengal remains relatively fresh and warm due to substantial river runoff and high precipitation, while the Arabian Sea is notably saline as a result of high evaporation, especially during the summer monsoon season (Hood et al., 2024; Shetye et al., 1994; Varkey et al., 1996). The Arabian Sea and the Bay of Bengal are seasonally connected by the southwest and northeast monsoon currents, which advect heat and salinity between the basins (Rainville et al., 2022; Sanchez-Franks et al., 2019; Schott & McCreary, 2001). The Arabian Sea is prone to cyclones and plays a critical role in providing moisture to the Indian Summer Monsoon Rainfall (Dey & Döös, 2021). Recent studies have shown rapid warming across the Indian Ocean, with more pronounced warming in the western Indian Ocean and the Arabian Sea (D'Mello & Kumar, 2018; Roxy et al., 2014, 2020; Swapna et al., 2013). This warming has caused changes in monsoon patterns and increased cyclone activity (Deshpande et al., 2021; Joseph et al., 2024; Pradhan et al., 2025; Roxy et al., 2015; Skliris

Visualization: Ligin Joseph
Writing – original draft: Ligin Joseph
Writing – review & editing: Ligin Joseph, Dipanjan Dey, Nikolaos Skliris, Alejandra Sanchez-Franks, Robert Marsh, Joel Hirschi, Sreevathsa Golla

et al., 2022; Yadav & Roxy, 2019). However, the exact mechanisms behind this rapid warming remain a subject of debate. Therefore, understanding the dynamics of the Arabian Sea is essential both for advancing scientific knowledge and addressing critical socio-economic implications.

The rising sea surface temperature (SST) across the Indian Ocean has gained significant attention in recent years. Roxy et al. (2014) demonstrated that the western tropical Indian Ocean has been experiencing a century-long warming trend, surpassing the warming rates of other tropical ocean regions. They attributed this trend to the asymmetry in the El Niño–Southern Oscillation (ENSO) teleconnection and the increased positive SST skewness associated with ENSO in recent decades. Swapna et al. (2013) connected this accelerated SST warming in the central equatorial Indian Ocean to the weakening of the summer monsoon's cross-equatorial flow. Additional studies have suggested that this warming may also be linked to the increased transport of warm water from the Pacific Ocean's warm pool into the Indian Ocean via the Indonesian Throughflow (ITF) (Chatterjee et al., 2024; McMonigal et al., 2022; Oppo & Rosenthal, 2010; Y. Zhang et al., 2018).

In addition to surface warming, the subsurface layers of the Arabian Sea are also exhibiting significant warming trends (Albert et al., 2023; Mathew et al., 2018; Nisha et al., 2023; Shee et al., 2023). Shee et al. (2023) used Argo data to show that the subsurface waters are experiencing the most intense warming and salting trends in the Arabian Sea. Albert et al. (2023) reported that the warming is more pronounced in the deeper regions of the Arabian Sea compared to the upper layers, and this trend is relatively more intense than in the Bay of Bengal. Their analysis revealed a strong negative correlation between upper ocean heat content (OHC) and Outgoing Longwave Radiation over the past two decades. Furthermore, they linked the increased OHC to the strengthening of downwelling Kelvin wave propagation. The study also found that the rise in surface heat fluxes and the reduction in vertical entrainment significantly contributed to warming in the southeastern Arabian Sea. Contrarily, Pratik et al. (2018) identified a declining trend in net surface heat flux into the ocean during the summer monsoon season, attributing subsurface warming to downwelling induced by an anomalous anti-cyclonic wind stress curl, which deepens the thermocline. They found that these changes in the wind stress curl are associated with a northward shift in the summer monsoon winds. Additionally, Nisha et al. (2023) demonstrated that warming in the upper 300 m of the Arabian Sea is influenced by the frequency of positive Indian Ocean Dipole (IOD) and El Niño events. They further suggested that subsurface heat accumulation below the mixed layer primarily drives warming in spring and summer, whereas heat stored within the mixed layer dominates during fall and winter.

The warming of the Arabian Sea has significant implications for the southwest monsoon rainfall over Southeast Asia (Joseph et al., 2024; Roxy et al., 2015; Skliris et al., 2022; Yadav & Roxy, 2019). Roxy et al. (2015) demonstrated that Indian Ocean warming weakens monsoon winds by altering the land-sea thermal gradient. J. Zhang et al. (2022) showed that Arabian Sea warming contributes to a westward shift in the Indian Summer Monsoon circulation. Li et al. (2022) highlighted that Arabian Sea warming enhances intraseasonal rainfall over the northeastern Arabian Sea, which drives an increasing trend in extreme rainfall over central-western parts of the Indian subcontinent. Kajakokulan et al. (2023) found that rapid Arabian Sea warming has led to increased summer monsoon rainfall over Sri Lanka.

In addition to its influence on monsoon dynamics, recent studies have also highlighted the impact of Arabian Sea warming on cyclonic activity. Rajeevan et al. (2013) demonstrated that the intensity of pre-monsoon tropical cyclones in the Arabian Sea is increasing, driven by a rising trend in tropical cyclone heat potential. Deo et al. (2011) observed that warming in the northern Arabian Sea supports enhanced cyclogenesis, while Deshpande et al. (2021) reported a 52% increase in the frequency of tropical cyclones in the Arabian Sea in recent years, attributed to regional warming.

These findings underscore the urgent need to understand the physical mechanisms driving the warming of the western Indian Ocean and the Arabian Sea, given its implications for regional monsoons, extreme rainfall, and cyclonic activity. Although previous studies collectively indicate an increasing trend in upper OHC in the Arabian Sea, the mechanisms driving this trend remain debated, with conflicting hypotheses in the literature. Notably, recent changes in OHC during the past decade (2014–2023) have not been adequately explored. One potentially important—but underexamined—mechanism involves the Great Whirl, a large, semi-permanent anticyclonic eddy that forms annually in the western Arabian Sea during the summer monsoon. Driven by strong southwesterly winds, it is one of the most energetic mesoscale features in the Indian Ocean, spanning several hundred kilometers and reaching depths exceeding 1,000 m (Beal & Donohue, 2013). The Great Whirl modulates upper-ocean

dynamics by altering heat storage, lateral heat transport, and the vertical structure of the thermocline (Beal & Donohue, 2013; Fischer et al., 1996; Jebri et al., 2024). Through its influence on downwelling, it can significantly reshape regional patterns of heat accumulation and biological productivity (Fischer et al., 1996; Jebri et al., 2024). While its circulation and associated downwelling have been documented, the impact of recent changes in its transport and location on Arabian Sea heat content remains poorly understood. This study addresses this gap by investigating the drivers of recent OHC changes in the western Indian Ocean, with a particular focus on heat accumulation during winter and summer monsoon seasons. The emphasis on OHC, rather than SST, is motivated by growing evidence of its importance in sustaining and intensifying tropical cyclones.

The structure of this paper is as follows: Section 2 describes the data and methods. Section 3 presents the results, including trends in OHC, net heat flux, and heat accumulation during the winter and summer monsoons. Finally, the paper concludes with a discussion and summary.

2. Data and Methods

2.1. Data Sets Used

This study utilizes oceanic reanalysis data sets. Monthly data for OHC in the upper 300 m, net downward heat flux at the sea surface (NHF), potential temperature, 20-degree isotherm depth (20D), sea surface height (SSH), zonal and meridional current velocities, and zonal and meridional wind stress are obtained from the global ocean and sea-ice reanalysis (ORAS5: Ocean Reanalysis System 5) (Copernicus Climate Change Service, 2021). The OCEAN5 reanalysis system uses the Nucleus for European Modeling of the Ocean (NEMO) ocean model and the NEMOVAR ocean assimilation system (Copernicus Climate Change Service, 2021). The choice of ORAS5 data is based on its demonstrated performance as one of the best-performing reanalysis data sets for analyzing tropical Indian Ocean circulation (Deepika et al., 2024). In addition, the UK Met Office Hadley Center Enhanced Ocean Data Assimilation and Climate Prediction (ENACT), archive version 4 (EN4), is used here, consisting of objectively-analyzed gridded monthly 3-D temperature data to produce an observationally-based estimate of OHC change over the considered period (Good et al., 2013).

2.2. Heat Transport Calculation

The heat transport through a zonal or meridional section is calculated using the following equation:

$$H = \int_{z_1}^{z_2} \int_{x_1}^{x_2} \rho\, C_p\, T\, v\, dx\, dz \tag{1}$$

where H is the heat transport (in W), ρ is the seawater density, taken as 1,026 kg/m^3, C_p is the specific heat capacity of seawater, taken as 3,996 J/(kg · °C), T is the potential temperature (in °C), v is the velocity component normal to the section (in m/s), x is the horizontal coordinate (longitude or latitude depending on the section orientation), and z is the vertical depth. The integration is performed over the specified horizontal extent (x_1 to x_2) and vertical depth range (z_1 to z_2) of the section. Since ORAS5 calculates OHC using temperature in degrees Celsius, relative to a reference temperature of 0°C following standard oceanographic convention, heat transport is also computed using potential temperature in degrees Celsius to ensure consistency with this approach.

Although several studies suggest that heat transport should be computed under the assumption of net-zero mass flux across a boundary, we did not explicitly enforce this condition. Our objective is to quantify the actual heat exchange through the section in the upper 300 m, rather than to construct a closed heat budget. Additional analyses were performed, where necessary, to ensure that the estimated increase in heat transport derived from this approach is both physically meaningful and consistent. While we focus on the upper 300 m layer, similar results are obtained when we define the control volume with an isopycnal layer as the bottom boundary (Figure S1 in Supporting Information S1).

2.3. OHC Budget

To enable direct comparison between 0 and 300 m OHC changes, surface fluxes, and lateral heat transport, we formulate the OHC budget as:

$$\Delta\left(\frac{\partial \mathrm{OHC}}{\partial t}\right) \approx \Delta\mathrm{NHF} + \frac{\Delta\mathrm{HT}}{A} + r, \tag{2}$$

where $\Delta(\partial \mathrm{OHC}/\partial t)$ is the change in OHC tendency between the two periods, estimated as the difference between the linear trend slopes of yearly OHC values in 1981–2013 and 2014–2023. We use slopes rather than time-mean derivatives to provide a robust measure of the long-term storage rate, which avoids contamination by strong seasonal and interannual variability. The OHC trend, originally expressed in GJ m^{-2} yr^{-1}, is converted to W m^{-2} by multiplying by 10^9 (J/GJ) and dividing by the number of seconds in a year ($\sim 3.15 \times 10^7$ s). ΔNHF is the change in net surface heat flux (2014–2023 minus 1981–2013), ΔHT is the change in net lateral heat transport across the southern boundary of the Arabian Sea, A is the area of the Arabian Sea, and r represents unresolved processes, including vertical heat exchange across 300 m.

2.4. Geostrophic Currents From SSH

To compute geostrophic currents, we use SSH and apply the geostrophic balance away from the equator:

$$u_g = -\frac{g}{f}\frac{\partial \eta}{\partial y}, \qquad v_g = \frac{g}{f}\frac{\partial \eta}{\partial x}, \tag{3}$$

where u_g and v_g are the zonal and meridional geostrophic velocities, η is SSH, g is gravitational acceleration, and $f = 2\Omega \sin \phi$ is the Coriolis parameter. A $\pm 1°$ equatorial band is masked where f becomes small.

2.5. Trend and Statistical Significance Test

The trends are calculated using the ordinary least squares (OLS) linear regression method. The statistical significance of the trend is then assessed using the two-tailed t-test, with the null hypothesis that there is no trend and an alternative hypothesis that the trend is non-zero. This approach detects significant trends in both directions, regardless of the sign of the trend. To account for temporal autocorrelation, which is particularly important for OHC due to the long memory of the ocean, the effective degrees of freedom at each grid point were estimated following Quenouille (1952):

$$N_{\mathrm{eff}} = N\frac{1 - r_1}{1 + r_1}, \quad \mathrm{DOF} = N_{\mathrm{eff}} - 2, \tag{4}$$

where N is the number of years and r_1 is the lag-1 autocorrelation of the regression residuals. The resulting effective DOF was then used in the t-test.

3. Results

3.1. Trends in the Ocean Heat Content

The annual mean and trend of OHC (referring to the upper 300 m throughout this study unless specified otherwise) during 2000–2023 in the tropics are presented in Figure 1. The choice of the upper 300 m OHC is based on our analysis, which shows that approximately 35% of the total full-depth ocean warming in the western Indian Ocean is stored within this layer. This upper ocean layer is also closely linked to the atmosphere; therefore, changes in OHC within this depth significantly impact ocean–atmosphere interactions. A notable and widespread increasing trend in OHC is observed in the western Indian Ocean, making it the only region within the tropics to exhibit such a widespread and significant positive trend (Figure 1b). Similar results were obtained using temperature data from the observationally-based EN4 data set, suggesting that this trend is not specific to a particular data set (Figure 1c). This emphasizes the need to analyze the mechanisms driving these trends to gain a deeper understanding of the underlying physical processes. The time series of yearly OHC averaged over the Arabian Sea (8.5°N–25°N, 50°E–77°E; black box in Figure 1b) reveals a decline in OHC toward the end of the 20th century, followed by a significant increasing trend of 0.87 GJ/m^2 over 24 years during the 21st century. Previous studies have attributed this earlier dip in OHC to a climate regime shift (Nisha et al., 2023; Swanson & Tsonis, 2009).

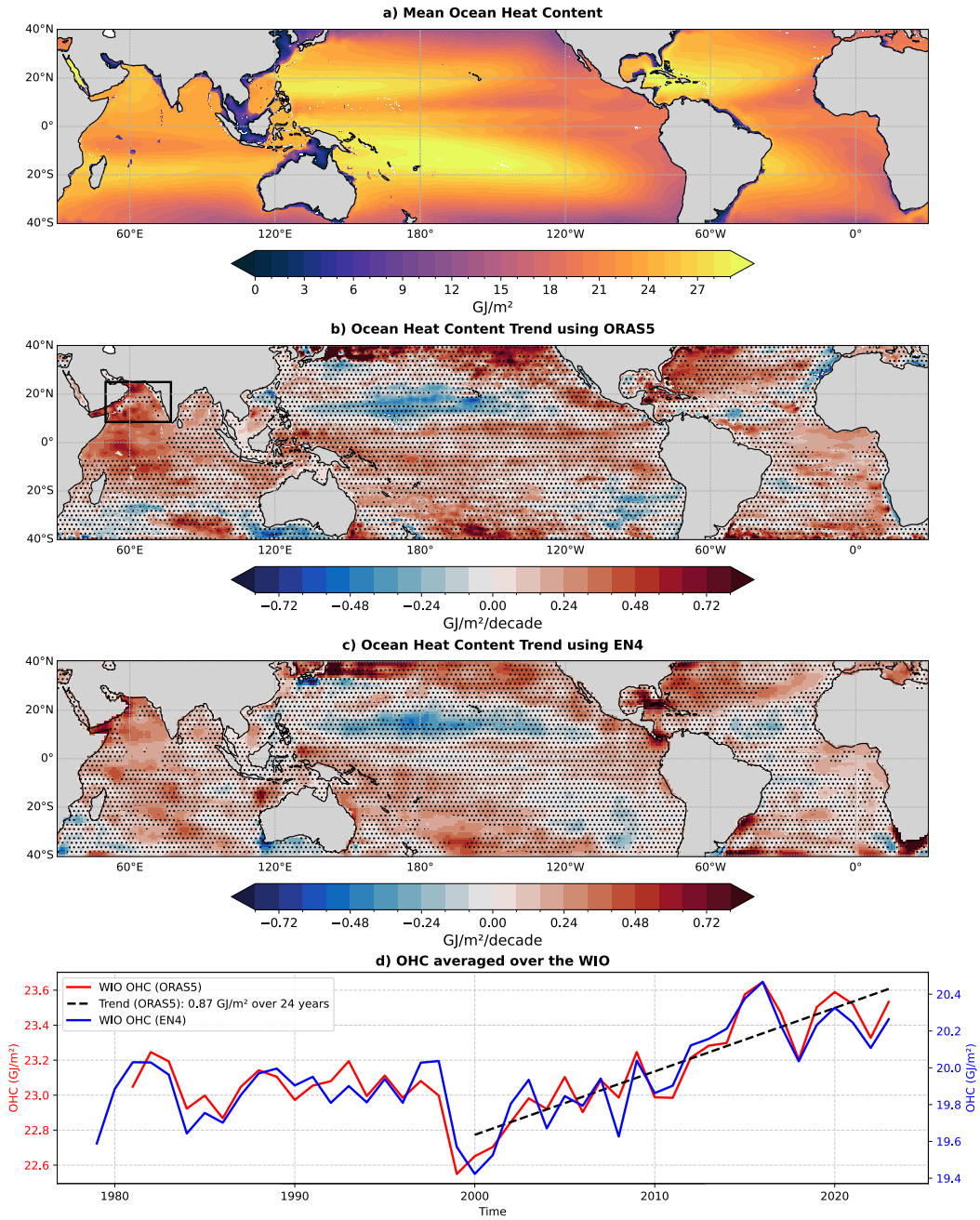

Figure 1. Ocean heat content (OHC) mean and trend. (a) The annual climatology of the upper 300 m OHC over the tropics. (b) Trends in the upper 300-m OHC during 2000–2023. The hashed regions indicate values that are not significant at the 95% confidence level. The black box (8.5°N–25°N, 50°E–77°E) highlights the Western Indian Ocean (WIO) region where the OHC trend is significant. Panel (c) same as (b), but using the EN4 data set. (d) The time series of the yearly OHC averaged over the WIO region (black box in panel b).

Changes in OHC are primarily driven by variations in net heat flux into the ocean and oceanic dynamics such as advection and vertical processes (Karlowska et al., 2024; Roberts et al., 2017). This study examines these processes in detail, starting with an analysis of net surface heat flux.

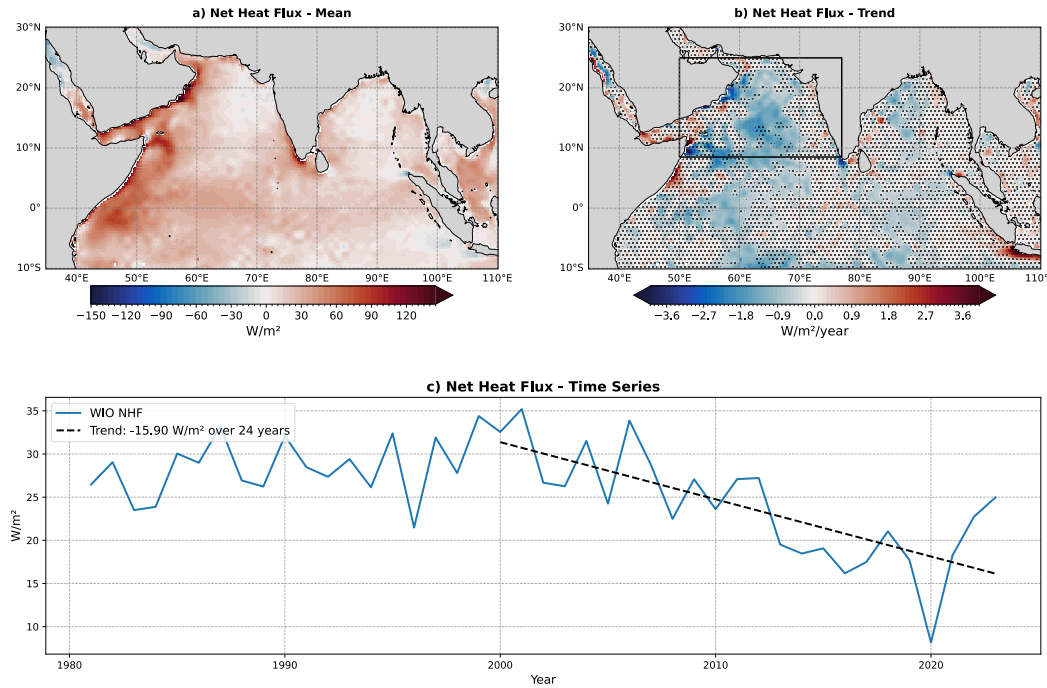

Figure 2. Net Heat Flux (NHF) mean and trend. (a) The annual climatology of the NHF (positive downwards). (b) Trends in the NHF during 2000–2023. The hashed regions indicate values that are not significant at the 95% confidence level. The black box (8.5°N–25°N, 50°E–77°E) highlights the Western Indian Ocean (WIO) region where the ocean heat content trend is significant. (c) The time series of the yearly NHF averaged over the WIO region (black box in panel b).

3.2. Trends in Net Heat Flux

The spatial mean, trends, and time series of the NHF averaged over the Arabian Sea are shown in Figure 2. The NHF exhibits a significant decreasing trend across most regions of the Arabian Sea. Recent studies have indicated a significant increase in evaporation over this region, suggesting that the latent heat flux may be the primary contributor to the observed decrease in NHF (Joseph et al., 2024; Pratik et al., 2018). This indicates that the ocean is releasing heat into the atmosphere and, consequently, becoming cooler. However, this is in contrast to the increasing OHC trend, implying that the NHF is not the primary driver of the observed rise in OHC.

3.3. The Role of Oceanic Transport

Given that the NHF does not account for the increasing trend in OHC in the Arabian Sea, an alternative driver could be the horizontal transport of heat. To investigate this, Table 1 shows the mean OHC, trend in OHC, and mean NHF averaged over the Arabian Sea (8.5°N–25°N, 50°E–77°E), along with the heat transport (calculated using Equation 1) across the zonal cross-section (50°E–77°E) at 8.5°N, averaged over two periods: 1981–2013 and 2014–2023.

Table 1
Ocean Heat Content (OHC) Mean, OHC Trend, and Net Heat Flux (NHF) Mean, Averaged Over the Arabian Sea (8.5°N–25°N, 50°E–77°E), Along With the Net, Northward, and Southward Heat Transport Through the Zonal Section (50°E–77°E) at 8.5°N, for the Periods 1981–2013 and 2014–2023

Time period	OHC (GJ/m^2)	OHC trend (W/m^2)	NHF (W/m^2)	Mean meridional heat transport (TW)	Northward heat transport (TW)	Southward heat transport (TW)
1981–2013	23.01	−0.02	28.08	−132	2,603	−2,735
2014–2023	23.46	+0.95	18.41	−58	2,702	−2,760
Difference	+0.45	+0.97	−9.67	+74	+99	−25

Table 2
Seasonal Heat Transport Along the Southern Boundary of the Arabian Sea (8.5°N) During Different Time Periods

Time period	Season	Net meridional heat transport (TW)	Northward heat transport (TW)	Southward heat transport (TW)
1981–2013	Winter Monsoon	836	2,040	−1,204
	Summer Monsoon	−1,373	3,670	−5,043
2014–2023	Winter Monsoon	1,059 (+223)	2,405 (+365)	−1,346 (−142)
	Summer Monsoon	−1,279 (+94)	3,460 (−210)	−4,739 (+304)

Note. The values in the bracket indicate the changes in the recent decade compared to the 1981–2013 mean.

As shown in Table 1, the mean OHC over the Arabian Sea increased by 0.45 GJ m^{-2} during 2014–2023 relative to the 1981–2013 mean. Given the area of the Arabian Sea (~3.27 million km^2), this corresponds to a total energy gain of approximately 1.61×10^{21} J, highlighting a substantial accumulation of heat with important implications for regional ocean–atmosphere interactions. The OHC trend, interpreted as the long-term OHC tendency (expressed in W m^{-2}; see Section 2.3 for details), shows a weak and statistically insignificant decrease during 1981–2013, followed by a significant positive trend during 2014–2023.

In contrast, the NHF into the Arabian Sea decreased by 9.6 W m^{-2} (a 34% reduction), implying a net surface heat loss. The net meridional heat transport across the southern boundary of the Arabian Sea (8.5°N, 50–77°E) remains southward (outward), but its magnitude has weakened by 74 TW, equivalent to a heat convergence of 22.6 W m^{-2} when normalized by the basin area. Decomposition of the meridional transport into northward and southward components shows that both increased in magnitude, but the northward inflow strengthened more than the outflow (Table 1). This asymmetry results in a net accumulation of heat within the Arabian Sea, consistent with the observed OHC increase. Reconciling the OHC rise with the surface heat loss requires a total heat input of approximately 10.6 W m^{-2} (0.97 + 9.67). Of this, 22.6 W m^{-2} is supplied by horizontal heat convergence through the southern boundary, with the remaining excess likely balanced by unresolved processes, including vertical redistribution of heat associated with downwelling and upwelling variability, mesoscale eddy activity, and other dynamical adjustments.

Given the seasonal reversal of ocean circulation in the Indian Ocean (see Schott et al. (2009) for a detailed review; mean currents are also shown in Figure S2 in Supporting Information S1), it is essential to examine the meridional transport on a seasonal basis. Table 2 presents the seasonal heat transport across the southern boundary during the winter monsoon (January–March) and summer monsoon (June–September) periods.

During the winter monsoon season, the currents flow northward toward the Arabian Sea, whereas during the summer monsoon, the current reverses, with the mean flow directed southward. From Table 2, comparing the recent decade (2014–2023) with the long-term mean (1981–2013), it is evident that the Arabian Sea experienced a net increase in heat accumulation during both the winter (223 TW) and summer (94 TW) monsoon seasons. In winter, this increase is primarily driven by a substantial rise in northward heat transport (365 TW), while the southward transport increased only modestly (142 TW). In contrast, during the summer monsoon, although the incoming heat transport decreased (210 TW), the outgoing southward transport decreased even more significantly (304 TW), resulting in net heat accumulation.

In the next section, the key drivers of this heat accumulation in the Arabian Sea during the winter and summer monsoon seasons are examined.

3.4. Heat Accumulation During the Winter Monsoon Season

To investigate the drivers of the increased heat transport into the Arabian Sea, the winter monsoon mean currents averaged over the upper 300 m, along with their difference for the period 2014–2023 relative to 1981–2013, are shown in Figure 3. Comparable results are obtained for the heat transport integrated to 300 m, which are presented in Figure S4 in Supporting Information S1.

From Figure 3b, it is evident that the westward current from the eastern Indian Ocean to the western Indian Ocean (Northeast Monsoon Current (NEC)), along the tip of India, has strengthened in the last decade. This intensification has the potential to transport more heat into the western Indian Ocean. Figure 4 presents the time series of

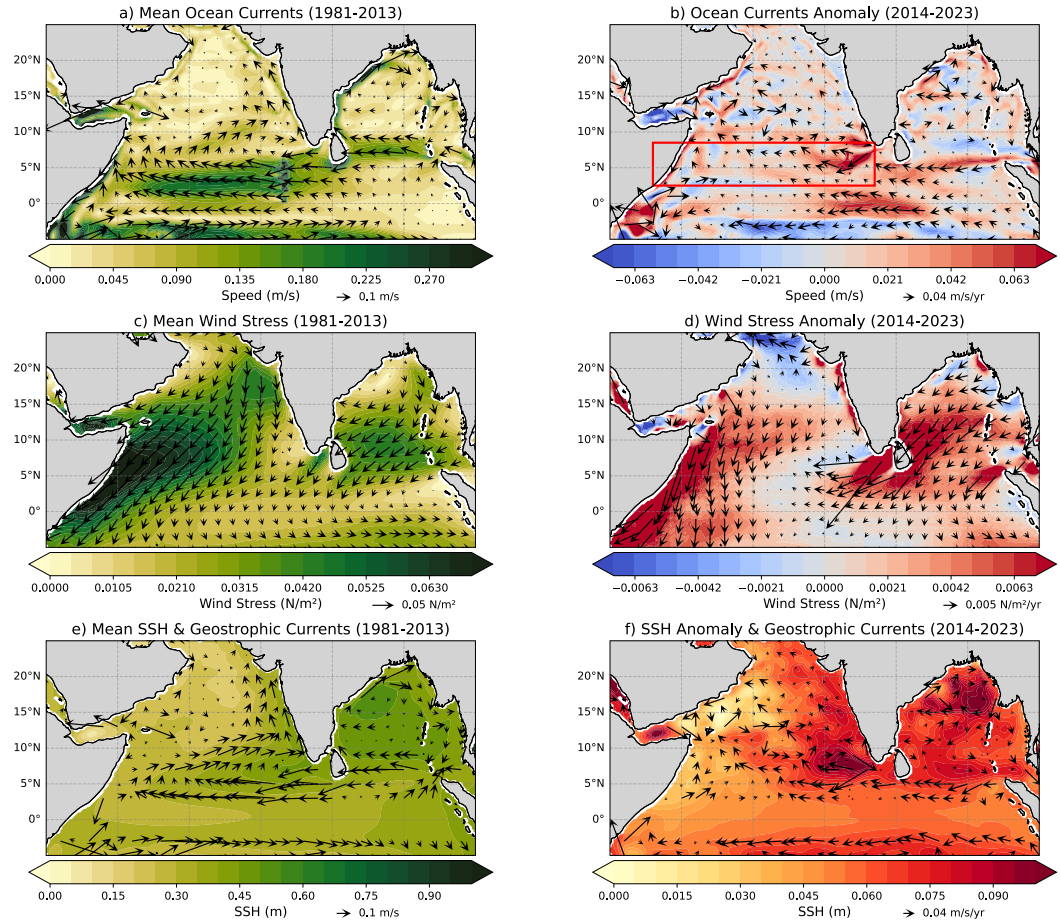

Figure 3. Winter monsoon season ocean currents and wind stress mean and difference. (a) The winter monsoon climatology of the 300 m averaged ocean currents. (b) Winter monsoon ocean currents difference for the period 2014–2023 relative to 1981–2013. The red box is used to calculate the heat transport from the eastern Indian Ocean to the western Indian Ocean. (c) The winter monsoon climatology of the wind stress. (d) Winter monsoon wind stress difference for the period 2014–2023 relative to 1981–2013. (e) The winter monsoon climatology of the sea surface height (SSH) and geostrophic currents. (f) Winter monsoon SSH and geostrophic currents difference for the period 2014–2023 relative to 1981–2013.

westward volume and heat transport along the meridional section at 77°E (1.5°S–8.5°N) and the zonal section at 8.5°N (46°E–77°E), which represent the eastern and northern boundaries of the box shown in Figure 3b, respectively, during the winter monsoon season. An increasing trend is observed in both westward volume and heat transport into the western Indian Ocean (Figures 4a and 4b). This heat is subsequently transported northward into the Arabian Sea, as indicated by the increasing trend in northward transport (Figures 4c and 4d).

The means (1981–2013 and 2014–2023) and difference (2014–2023 minus 1981–2013) of the vertical cross-section of the zonal and meridional velocity at 77°E and 8.5°N, respectively, during the winter monsoon are shown in Figure 5. Similar results are obtained for the vertical cross-section of heat transport which are presented in Figure S6 in Supporting Information S1. The zonal velocity cross-sections at 77°E indicate that the mean flow is westward in the upper ocean and eastward below 100 m near the equator (Figures 5a and 5b). The eastward flow near the equator below 70 m depth is the Equatorial Undercurrent (EUC), which reaches its maximum strength during February–March and subsequently weakens (Chen et al., 2015; Gnanaseelan & Deshpande, 2017). The zonal velocity difference (Figure 5c) exhibits negative values, particularly in the upper 150 m, suggesting an intensification (weakening) of westward (eastward EUC) flow in the last decade. Similarly, the mean meridional velocity at 8.5°N is predominantly northward, which corresponds to the surface Ekman flow (Figures 5d and 5e; Schott et al., 2009). The meridional velocity difference (Figure 5f) shows positive values, indicating that the northward flow has strengthened and deepened over the last decade.

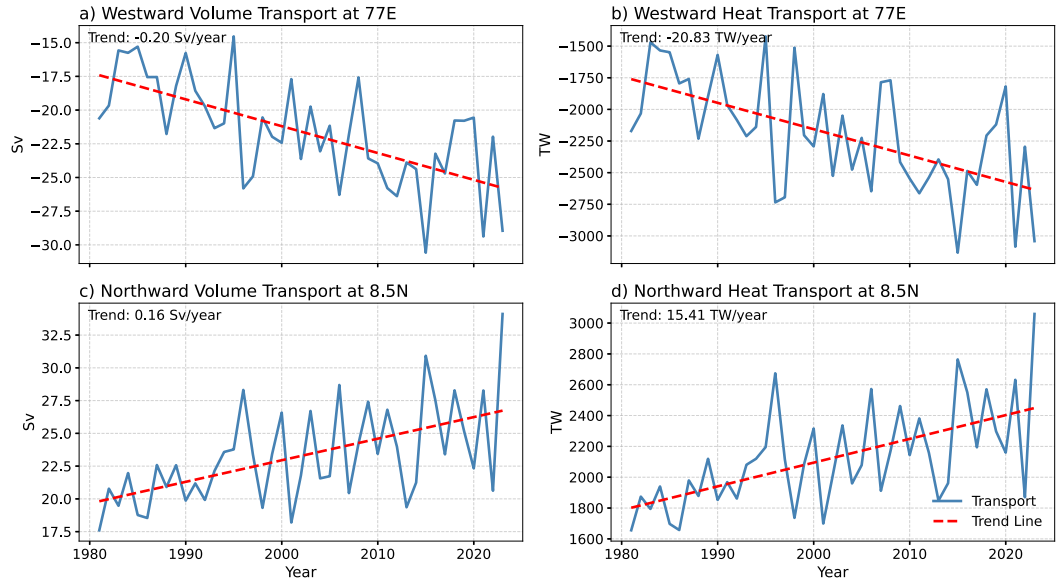

Figure 4. Time series of upper 300 m volume and heat transport during the winter monsoon season. (a) Westward volume transport along the meridional section at 77°E (1.5°S–8.5°N), representing the eastern boundary of the box shown in Figure 3b. Panel (b) same as (a) but for heat transport. (c) Northward volume transport along the zonal section at 8.5°N (46°E–77°E), representing the northern boundary of the box shown in Figure 3b. Panel (d) same as (c), but for heat transport.

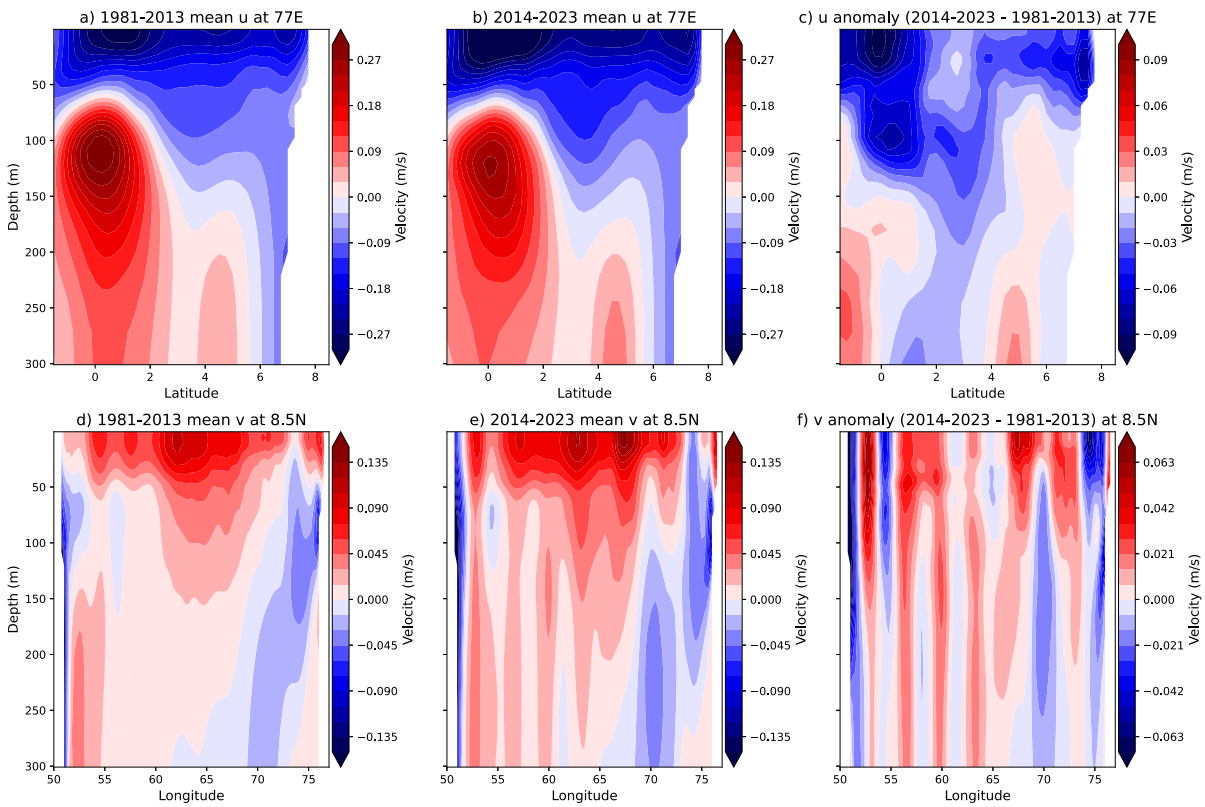

Figure 5. Vertical cross-section of velocity during winter monsoon. (a) Vertical cross-section of the 1981–2013 mean zonal velocity along the meridional section at 77°E (1.5°S–8.5°N), representing the eastern boundary of the box shown in Figure 3b. Panel (b) same as (a) but for the 2014–2023 mean. (c) Zonal velocity difference (b–a). (d) Vertical cross-section of the 1981–2013 mean meridional velocity along the zonal section at 8.5°N (50°E–77°E), representing the northern boundary of the box shown in Figure 3b. Panel (e) same as (d) but for the 2014–2023 mean. (f) Meridional velocity difference (e–d).

Furthermore, the net heat transport along the section at 77°E (1.5°S–8.5°N), representing the eastern boundary of the box in Figure 3b, is calculated as −709 TW for the period 1981–2013 (negative values indicate westward transport). Over the last decade, this has increased to −1,237 TW, implying an additional westward heat transport of 528 TW (74% increase). However, this increase does not necessarily mean that all of this heat is transported northward into the Arabian Sea; some may instead be diverted southward. To investigate this, the meridional heat transport at 1.5°S (40°E–77°E), representing the southern boundary of the box in Figure 3b, is analyzed. The net heat transport at this boundary has increased from 742 TW (1981–2013 mean) to 797 TW in the last decade. This suggests that the heat entering the western Indian Ocean from the eastern Indian Ocean (+528 TW) is not primarily exiting through the south of the equator. Instead, a significant portion is being transported northward into the Arabian Sea (223 TW), with the remaining heat contributing to the increase in OHC within the region.

It is further observed that the anomalous westward (strengthening of the NEC) and northward currents are likely driven by anomalous wind stress over the Indian Ocean (Figure 3d). The wind stress induces Ekman transport to the west, thereby enhancing the westward current. To examine this, we computed the zonal Ekman transport anomaly at 77°E between 1.5°S and 8.5°N (excluding 1° around the equator) and present the results in Figure S3a in Supporting Information S1. A significant negative trend (increased westward transport) is evident; however, its magnitude is an order of magnitude smaller than the total 0–300 m transport trend (Figure 4b). This indicates that Ekman dynamics alone cannot account for the observed strengthening of the westward transport.

To diagnose the geostrophic contribution, we computed SSH and SSH-derived geostrophic currents (Figures 3e and 3f). The SSH anomalies exhibit a pronounced meridional gradient, with elevated SSH in the Bay of Bengal and southeastern Arabian Sea relative to the equatorial region. This strengthened north–south SSH slope has the potential to drive enhanced westward geostrophic flow, thereby increasing the westward volume and heat transport across 77°E. Close to the equator, where geostrophic balance weakens, additional ageostrophic westward flow is expected, reinforcing the response.

In addition, positive wind stress curl anomalies over the Indian Ocean could induce a northward transport via the Sverdrup relationship. The time series of 300-m volume transport and Sverdrup transport, calculated using equation 1S, is shown in Figure S3b in Supporting Information S1. The two estimates show good agreement, with both exhibiting significant positive trends during 2000–2023. This indicates that anomalous wind stress initiates a basin-scale adjustment that contributes to the enhanced northward flow. Furthermore, the SSH anomaly field displays a clear east–west gradient within the Arabian Sea, with higher SSH anomalies in the eastern basin and lower anomalies in the west. This positive zonal SSH slope induces an anomalous northward geostrophic flow, consistent with the SSH-derived geostrophic velocities (Figures 3e and 3f). The combination of Sverdrup-driven northward transport and SSH-gradient-driven geostrophic adjustment therefore reinforces the anomalous volume and heat transport into the Arabian Sea during the winter monsoon season.

3.5. Heat Accumulation During the Summer Monsoon Season

The mean ocean currents averaged over the upper 300 m, the mean wind stress, and their difference (2014–2023 minus 1981–2013) during the summer monsoon season, are shown in Figure 6. Comparable results are obtained for the heat transport integrated to 300 m, which are presented in Figure S5 in Supporting Information S1. The wind stress differences indicate a northward shift in the summer monsoon circulation. This observation aligns with the findings of Sandeep and Ajayamohan (2014), who demonstrated that the Indian summer monsoon low-level jet is shifting poleward due to global warming. Similarly, Pratik et al. (2018), using ORAS4 reanalysis data from 1979 to 2015, showed that this poleward shift in southwest monsoon winds enhances the anti-cyclonic wind stress curl, inducing downwelling and reducing the southward heat transport from the Arabian Sea. This phenomenon is observed in the current study as well (Figure 6d). This suggests that the mechanism proposed by Pratik et al. (2018) remains relevant and continues to operate during the most recent decade.

This study also reveals a reduction in the amount of heat exported from the Arabian Sea during the summer monsoon season (Table 2), supporting the mechanism proposed by Pratik et al. (2018). However, we found that most of these changes in heat transport are concentrated near the Great Whirl region. When the Great Whirl region is excluded, and heat transport is calculated along 8.5°N, 57°E–77°E, the southward transport shows an increasing change during the last decade: −2,441 TW during 1981–2013 and −2,529 TW during 2014–2023. In contrast, the southward heat transport along the Great Whirl region (8.5°N, 50°E–56°E) shows a sharply decreasing change: −2,532 TW during 1981–2013 and −2,111 TW during 2014–2023. Additionally, the northward heat transport in

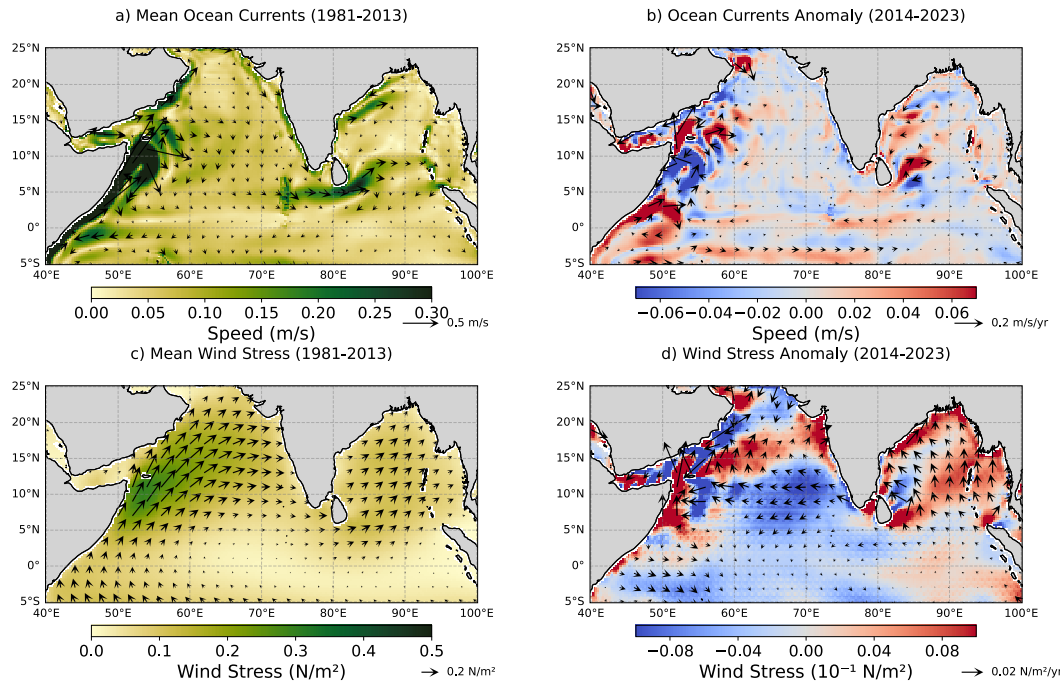

Figure 6. Summer Monsoon ocean currents and wind stress mean and difference. (a) The summer monsoon climatology of the 300 m averaged ocean currents. (b) Summer Monsoon ocean currents difference for the period 2014–2023 relative to 1981–2013. The red box is the usual location of the Great Whirl. (c) The summer monsoon climatology of the wind stress. (d) Summer Monsoon wind stress difference for the period 2014–2023 relative to 1981–2013.

this region has also decreased: 3057 TW during 1981–2013 and 2,814 TW during 2014–2023. While the northward transport branch of the Great Whirl has decreased by 243 TW, the southward branch has decreased even more significantly by 421 TW, resulting in an overall convergence of heat. These findings indicate that changes in the Great Whirl are the major contributor to the observed heat convergence during the summer monsoon in the Arabian Sea, particularly during the last decade.

The mean and 2000–2023 trends of the OHC, SSH, depth of the 20-degree isotherm (20D), and current speed during the summer monsoon season are shown in Figure 7. The trends during 2000–2023 exhibit similar patterns to the 2014–2023 differences (2014–2023 minus 1981–2013; not shown). Therefore, analyzing the trends provides insights similar to analyzing the differences from the last decade. However, trends also offer the advantage of indicating whether these changes are statistically significant.

The usual location of the Great Whirl is marked as a black box in Figure 7. The mean OHC in the Great Whirl region is high (Figure 7a), which can be attributed to downwelling caused by the anti-cyclonic circulation of the Great Whirl. This downwelling signal is also evident in the means of SSH and 20D (Figures 7c and 7e). However, the trends in current speeds (Figure 7h) indicate that the strength of the Great Whirl is decreasing. This weakening could result in reduced downwelling, as suggested by the trends in SSH and 20D (Figures 7d and 7f). The reduction in downwelling could also lead to a decrease in OHC, which is reflected in the negative (though non-significant) trends in OHC within the usual Great Whirl location (Figure 7b). Interestingly, toward the north of the Great Whirl, the trends in OHC, SSH, 20D, and current speed all show positive values. This observation hints at a northward shift of the Great Whirl. The new location of the Great Whirl, near the Socotra Island region, which is typically characterized by upwelling, could now be experiencing reduced upwelling or even downwelling due to this shift, thereby influencing the OHC. This raises the question of whether the Great Whirl has indeed shifted northward, requiring further investigation.

To investigate possible changes in the latitude of the Great Whirl's center, the time series of its latitude is plotted in Figure 8a. The latitude of the Great Whirl's center is determined as the latitude of the maximum SSH within the region bounded by 50°E–56°E and 5°N–11°N during June–August. Figure 8a reveals a northward shift in the

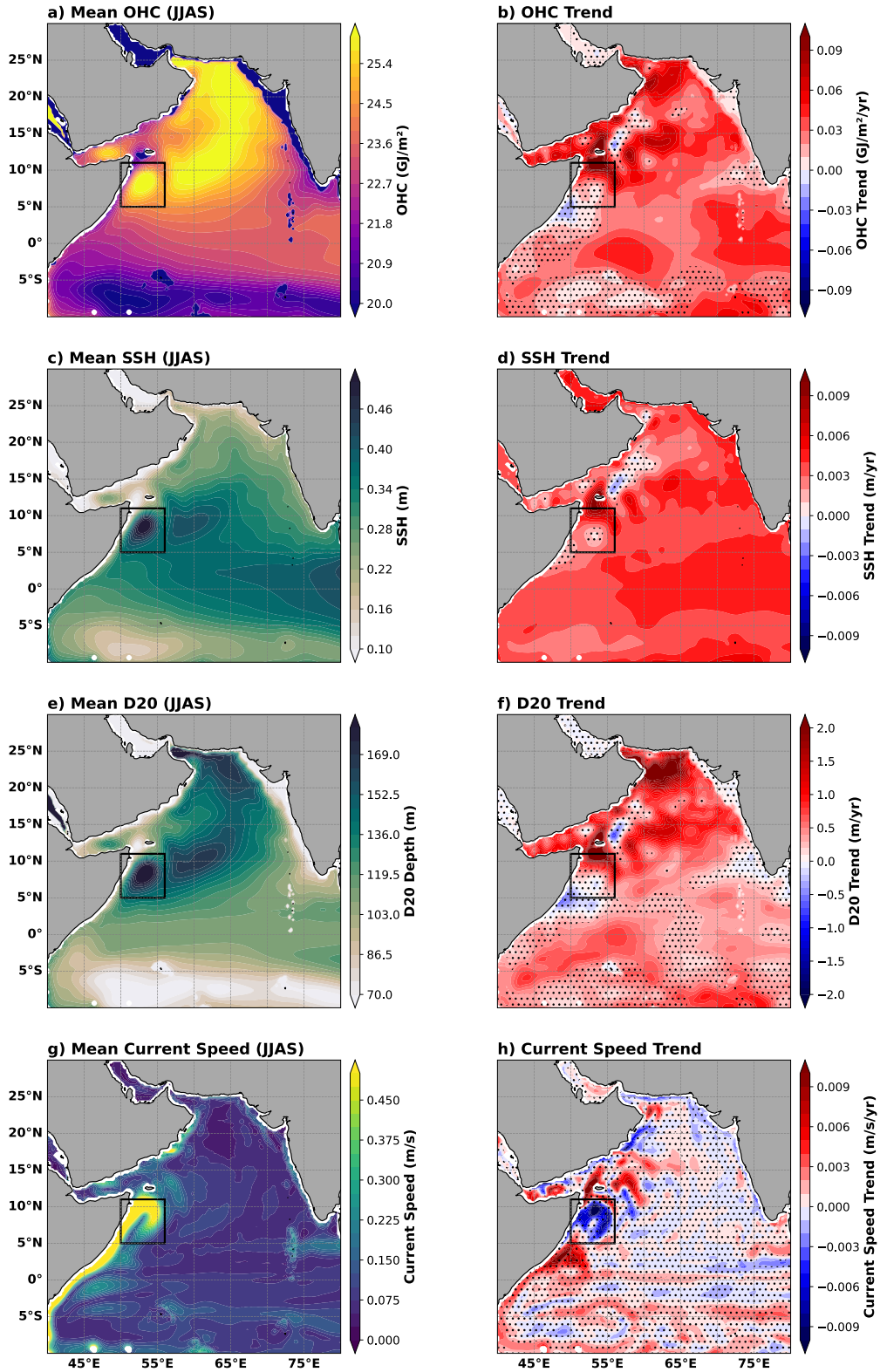

Figure 7. The ocean heat content (OHC), sea surface height (SSH), 20D and current speed during the summer monsoon season. (a) Mean OHC during the monsoon season. (b) OHC trend during 2000–2023. (c) Mean SSH during the monsoon season. (d) SSH trend during 2000–2023. (e) Mean 20D during monsoon. (f) 20D trend during 2000–2023. (g) Mean current speed averaged over 300 m during the monsoon. (h) Currents speed trend during 2000–2023. The hashed regions indicate values that are not significant at the 95% confidence level. The black box represents the mean location of the Great Whirl.

latitude of the Great Whirl's center, which is particularly pronounced during the last decade. Furthermore, the latitude-depth cross-section of the mean and trend of temperature, averaged over 50°E–56°E (Figures 8b and 8c), shows the steepest thermocline near Socotra Island (10°N–12°N), confirming it as an upwelling region. The temperature trend in this region indicates a significant increase, suggesting decreased upwelling plausibly caused by the northward shift of the Great Whirl. This subsurface warming can be advected to other longitudes, potentially contributing to broader subsurface warming in the Arabian Sea as shown in Figure 8e.

4. Summary and Concluding Remarks

This study demonstrates that the upper 300 m OHC exhibits a significant and widespread increasing trend in the western Indian Ocean during 2000–2023, in agreement with previous studies (Albert et al., 2023; Nisha et al., 2023; Pratik et al., 2018). Notably, this is the only region in the global tropical ocean where the OHC trend is both statistically significant and spatially extensive during this period. Despite this increase in OHC, the NHF into the ocean is decreasing, suggesting that local heat accumulation is driven more by oceanic processes than by direct atmospheric forcing. Previous studies (using ERA5 and Tropflux data sets) have attributed this decrease in NHF to increased evaporation over the Arabian Sea in recent decades (Joseph et al., 2024; Pratik et al., 2018). It is important to note that ORAS5 is forced by ERA-Interim data (1979–2014) and ECMWF NWP thereafter, which may influence surface flux calculations.

Our analysis reveals that the observed increase in OHC is primarily driven by heat accumulation in the western Indian Ocean, largely resulting from changes in heat transport along the southern boundary of the Arabian Sea. The Arabian Sea is landlocked in its north, and the heat transport from the Persian Gulf and the Red Sea (6–8 TW) is minimal compared to the transport along its southern boundary (130 TW). Furthermore, our results indicate that the heat accumulation is modulated by changes during both the winter and summer monsoon seasons. A schematic summary of the study is shown in Figure 9.

During the winter monsoon, an increasing trend is observed in both the volume and heat transport into the western Indian Ocean. This trend is primarily attributed to an anomalous westward transport from the eastern equatorial Indian Ocean, but our diagnostics indicate that the enhanced transport cannot be explained by wind-forced Ekman processes alone. Instead, a substantial part of the anomaly arises from changes in SSH, which alter the large-scale pressure gradients and therefore the geostrophic circulation. In particular, the SSH anomaly field exhibits a strengthened meridional gradient between the equatorial region and the Bay of Bengal–southeastern Arabian Sea, driving an intensified westward geostrophic flow. Simultaneously, a pronounced east–west SSH gradient within the Arabian Sea induces an anomalous northward geostrophic transport. Together, these SSH-driven adjustments reinforce the westward and northward currents, increasing the inflow of warm water into the Arabian Sea. Of the extra 528 TW (relative to the 1981–2013 mean) of heat transported into the western Indian Ocean over the last decade, 223 TW is directed north into the Arabian Sea, while the remainder contributes to the regional OHC increase. Although the southward export from the Arabian Sea also increases, it does not fully offset the enhanced northward geostrophic inflow, resulting in net heat accumulation. Finally, we note that the drivers of SSH variability likely involve a combination of wind-stress curl (through Ekman pumping) and thermosteric sea-level rise. Disentangling the relative contributions of these processes is non-trivial because wind stress influences SSH both locally and remotely via wave propagation, and warming-induced steric changes also modulate SSH. A detailed attribution of SSH changes would require numerical simulations, which are therefore beyond the scope of this study but represent an important direction for future work.

In summer, consistent with earlier studies, the poleward shift of southwest monsoon winds intensifies the anticyclonic wind stress curl, promoting downwelling and reducing southward heat export. However, our analysis reveals that these changes are concentrated near the Great Whirl region. When this region is excluded, southward heat transport exhibits an increasing trend over the last decade. While the northward branch of the Great Whirl has weakened, the southward branch has decreased even more significantly, leading to an overall convergence of heat. Additionally, the northward displacement of monsoon winds causes the Great Whirl to migrate closer to the Socotra Islands—a region typically dominated by upwelling. This shift enhances downwelling, potentially alters the regional OHC, and redistributes heat across the Arabian Sea. Our study provides evidence of this northward shift of the Great Whirl based on OHC, SSH, 20D, and wind speed trends, as well as by estimating the eddy center from SSH (a simplified method for identifying the Great Whirl's position). We note, however, that other methods

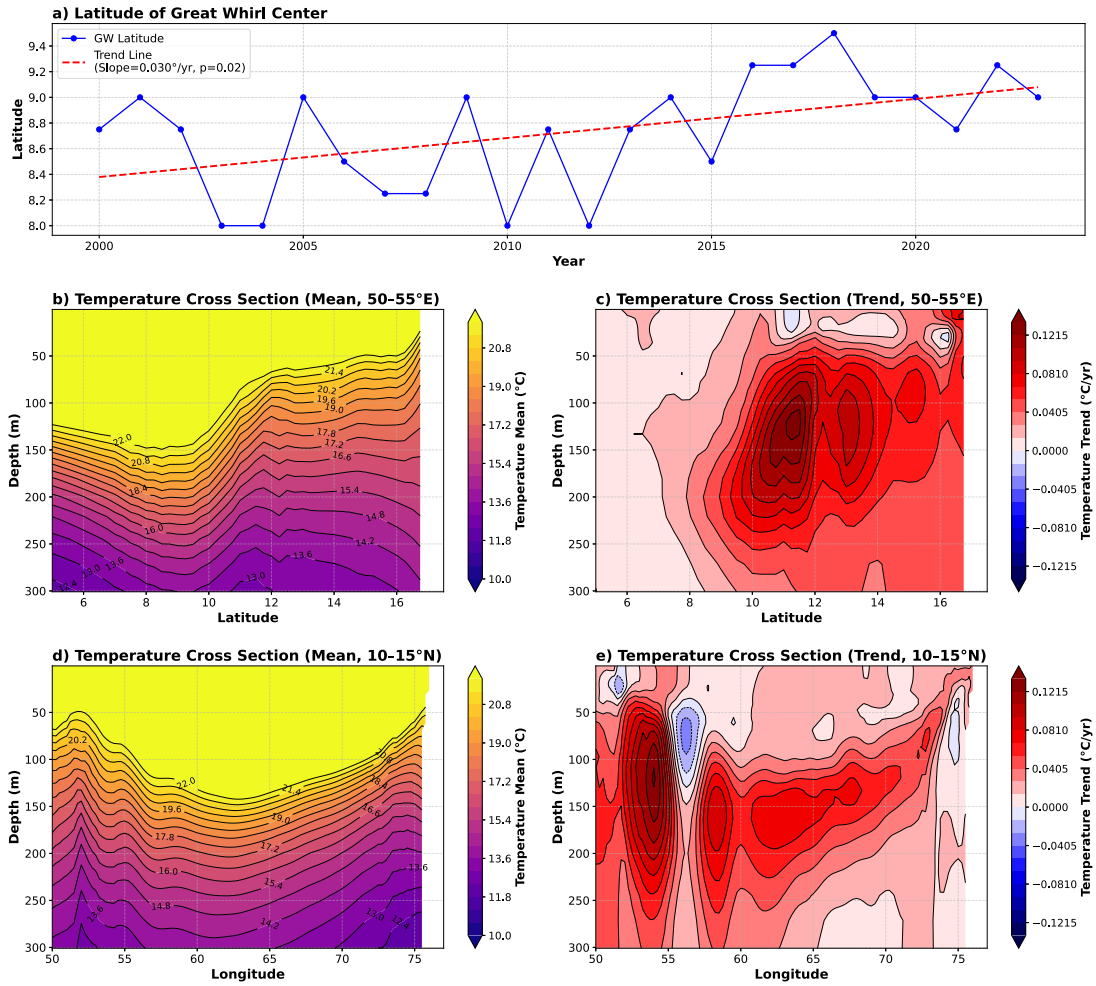

Figure 8. The northward shift of the Great Whirl during the summer monsoon. (a) The time series of the latitude of the Great Whirl center. The latitude of the Great Whirl's center is determined as the latitude of the maximum sea surface height (SSH) within the region bounded by 50°E–56°E and 5°N–11°N during June–August. The red dashed line shows the linear trend, with a slope of 0.030°/year, suggesting a northward shift of the Great Whirl. (b) The mean temperature cross-section (50°E–55°E) showing temperature distribution as a function of depth and latitude. (c) The temperature trends (2000–2023) for the same cross-section (50°E–55°E). (d) The mean temperature cross-section (10°N–15°N) showing temperature distribution as a function of depth and longitude. (e) The temperature trends (2000–2023) for the same cross-section (10°N–15°N).

exist for determining the eddy center, and the northward migration of the Great Whirl could be an interesting research topic in its own right. We therefore invite future studies to explore this in more detail.

Although anomalous subsurface warming near the Great Whirl may be advected and spread across the basin, wave dynamics can also play an important role. Positive wind stress anomalies between 12°N and 20°N in the Arabian Sea (Figure 6) can excite downwelling Rossby waves, contributing to thermocline deepening, similar to the mechanism discussed in Albert et al. (2023). Furthermore, Rossby waves generated in the Bay of Bengal can propagate westward, interact with the Indian coastline as coastal Kelvin waves, and subsequently radiate westward again as Rossby waves, potentially influencing subsurface heat distribution in the Arabian Sea (Albert et al., 2023). At the same time, several regions in the Arabian Sea exhibit negative wind stress anomalies, making the overall influence of wind stress spatially heterogeneous and uncertain. Nevertheless, the impact of wind stress-induced wave processes on subsurface warming and heat redistribution is worth considering alongside advection by the Great Whirl and could be a promising topic for future research in its own right.

As noted in Section 2, several studies recommend computing heat transport under the assumption of net-zero mass flux across a boundary, since otherwise the calculated transport may reflect temperature changes rather than actual heat transport. Moreover, an apparent increase in heat transport may result from a substantial rise in

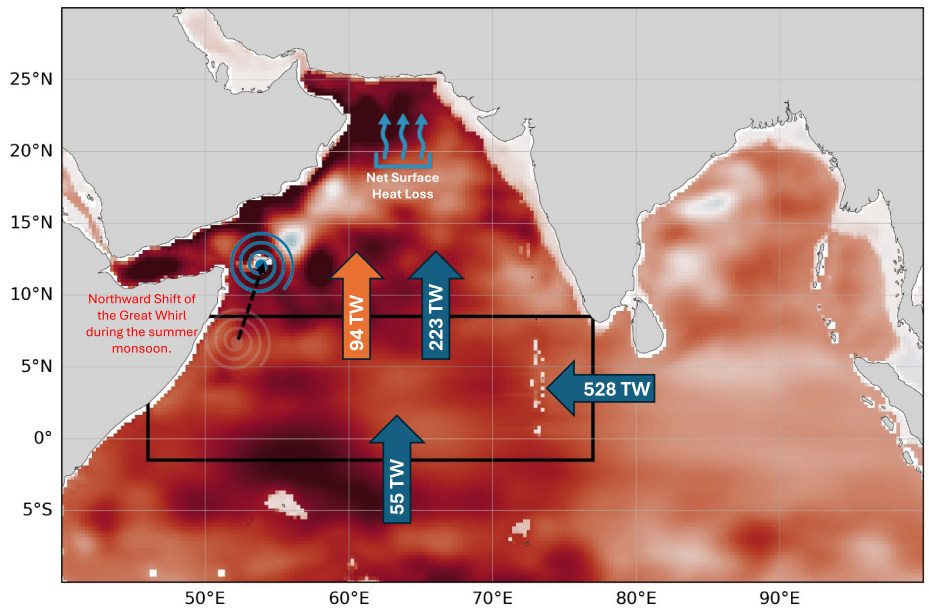

Figure 9. Schematic representation of the drivers of upper-ocean heat content (OHC) change in the western Indian Ocean. Shading shows the 300 m OHC trend during 2000–2023. Blue arrows denote anomalous heat transport during the winter monsoon and orange arrows during the summer monsoon, with values given as anomalies relative to the 1981–2013 mean (2014–2023 minus 1981–2013). The schematic also highlights net surface heat loss in the region and the northward displacement of the Great Whirl in summer.

water velocity accompanied by a slight decrease in temperature, indicating that more water, not necessarily more heat, is being transported. To investigate this, we computed the temperature of the inflow at 77°E and 8.5°S and compared it with the basin-averaged temperature (Figure S7 in Supporting Information S1). The inflow temperature was found to be substantially higher than the basin temperature, implying that increased volume or heat transport through this section could raise the basin's temperature. Therefore, we did not enforce the net-zero mass flux condition, as our objective was to quantify the actual heat exchange through the upper 300 m rather than to construct a closed heat budget. While we focus on the upper 300 m layer, we note that an alternative and more physically meaningful approach is to define the control volume using an isopycnal layer as the lower boundary. Such an approach can provide complementary insights into heat exchanges along material surfaces; however, our comparison with the isopycnal-based method (not shown) shows that the key transport and OHC signals are consistent between the two methods.

In addition to these findings, our results further underscore that the upper OHC in the western Indian Ocean is predominantly governed by oceanic heat transport rather than by net heat flux at the surface. For example, during the late 20th century, a sharp decline in OHC was observed despite persistently high NHF values (Figures 1 and 2). As shown in our inflow temperature analysis (Figure S7 in Supporting Information S1), this decline coincided with a sudden drop in inflow temperature, especially at 77°E, highlighting the role of lateral temperature advection in modulating OHC. Furthermore, although NHF shows a decreasing trend in recent decades, the OHC exhibits an increasing trend, reinforcing the notion that the rising OHC is more closely linked to oceanic heat convergence. It is also important to recognize that heat transport into the basin displays strong variability, and interannual climate phenomena such as ENSO and the IOD likely modulate this transport. A detailed analysis of these influences is beyond the scope of this study but presents an important avenue for future research.

The warming of the western Indian Ocean, and particularly the Arabian Sea, carries significant implications. Various studies have shown that the Arabian Sea is a major moisture source for the summer monsoon rainfall over southeast Asia, affecting millions of people (Dey & Döös, 2021). Additionally, the warming impacts cyclone activity in the region (Deo et al., 2011; Deshpande et al., 2021; Nisha et al., 2023; Pradhan et al., 2025; Rajeevan et al., 2013). Understanding the drivers of this warming is crucial, and our study offers hypotheses regarding the

mechanisms affecting the upper layers of the western Indian Ocean. Future studies employing idealized model experiments could further test these hypotheses and refine our understanding of these processes.

Conflict of Interest

The authors declare no conflicts of interest relevant to this study.

Data Availability Statement

The ORAS5 data set used in this study is available at Copernicus Climate Change Service (2021). The EN.4.2.2 data is available at Good et al. (2013).

Acknowledgments
This work was supported by the Natural Environmental Research Council (Grant NE/S007210/1). A.S-F. was supported by the NEW NORMAL project (https://noc.ac.uk/projects/new-normal) under NERC Grant NE/W003813/1. The authors would like to thank Lijo Abraham Joseph, Dr. Pascal Terray, Dr. Bieito Fernández Castro, and Dr. Duo Chan for helpful discussions. Additionally, AI tools such as Grammarly and ChatGPT were occasionally used mindfully to refine writing and Python code (Grammarly, 2024; OpenAI, 2024). This work used JASMIN, the UK collaborative data analysis facility. The authors also gratefully acknowledge the two anonymous reviewers whose constructive comments substantially improved the clarity and quality of this manuscript.

References

Albert, J., Gulakaram, V. S., Vissa, N. K., Bhaskaran, P. K., & Dash, M. K. (2023). Recent warming trends in the Arabian Sea: Causative factors and physical mechanisms. *Climate*, *11*(2), 35. https://doi.org/10.3390/cli11020035

Beal, L. M., & Donohue, K. A. (2013). The great whirl: Observations of its seasonal development and interannual variability. *Journal of Geophysical Research: Oceans*, *118*(1), 1–13. https://doi.org/10.1029/2012JC008198

Chatterjee, A., Sajidh, C. K., Murtugudde, R., McPhaden, M. J., Shenoi, S. S. C., & Vinayachandran, P. N. (2024). Rapid 21st century warming in the southern Indian Ocean driven by altered inter-basin connections. *Research Square*. https://doi.org/10.21203/rs.3.rs-4247247/v1

Chen, G., Han, W., Li, Y., Wang, D., & McPhaden, M. J. (2015). Seasonal-to-interannual time-scale dynamics of the equatorial undercurrent in the Indian Ocean. *Journal of Physical Oceanography*, *45*(6), 1532–1553. https://doi.org/10.1175/jpo-d-14-0225.1

Copernicus Climate Change Service. (2021). Oras5 global ocean reanalysis monthly data from 1958 to present [Dataset]. *ECMWF*. https://doi.org/10.24381/CDS.67E8EEB7

Deepika, P. B., Mohan, S., & Srinivas, G. (2024). Intercomparison of tropical Indian Ocean circulation in ocean reanalysis and evaluation in CMIP6 climate models. *Dynamics of Atmospheres and Oceans*, *106*, 101456. https://doi.org/10.1016/j.dynatmoce.2024.101456

Deo, A. A., Ganer, D. W., & Nair, G. (2011). Tropical cyclone activity in global warming scenario. *Natural Hazards*, *59*(2), 771–786. https://doi.org/10.1007/s11069-011-9794-8

Deshpande, M., Singh, V. K., Ganadhi, M. K., Roxy, M. K., Emmanuel, R., & Kumar, U. (2021). Changing status of tropical cyclones over the north Indian Ocean. *Climate Dynamics*, *57*(11–12), 3545–3567. https://doi.org/10.1007/s00382-021-05880-z

Dey, D., & Döös, K. (2021). Tracing the origin of the South Asian summer monsoon precipitation and its variability using a novel Lagrangian framework. *Journal of Climate*, *34*(21), 8655–8668. https://doi.org/10.1175/JCLI-D-20-0967.1

D'Mello, J. R., & Kumar, S. P. (2018). Processes controlling the accelerated warming of the Arabian Sea. *International Journal of Climatology*, *38*(2), 1074–1086. https://doi.org/10.1002/JOC.5198

Fischer, J., Schott, F., & Stramma, L. (1996). Currents and transports of the Great Whirl-Socotra Gyre system during the summer monsoon, August 1993. *Journal of Geophysical Research*, *101*(C2), 3573–3587. https://doi.org/10.1029/95JC03617

Gnanaseelan, C., & Deshpande, A. (2017). Equatorial Indian Ocean subsurface current variability in an ocean general circulation model. *Climate Dynamics*, *50*(5–6), 1705–1717. https://doi.org/10.1007/s00382-017-3716-8

Good, S. A., Martin, M. J., & Rayner, N. A. (2013). En4: Quality controlled ocean temperature and salinity profiles and monthly objective analyses with uncertainty estimates [Dataset]. *Journal of Geophysical Research: Oceans*, *118*(12), 6704–6716. https://doi.org/10.1002/2013JC009067

Grammarly. (2024). Grammarly [Software]. Retrieved from https://app.grammarly.com/

Hood, R. R., Ummenhofer, C. C., Phillips, H. E., & Sprintall, J. (2024). Chapter 1—Introduction to the Indian Ocean this book has a companion website hosting complementary materials. In C. C. Ummenhofer & R. R. Hood (Eds.), *The Indian Ocean and its role in the global climate system* (pp. 1–31). Elsevier. https://doi.org/10.1016/B978-0-12-822698-8.00015-9

Jebri, F., Srokosz, M., Raitsos, D. E., Jacobs, Z. L., Sanchez-Franks, A., & Popova, E. (2024). Absence of the great whirl giant ocean vortex abates productivity in the somali upwelling region. *Communications Earth & Environment*, *5*(1), 20. https://doi.org/10.1038/s43247-023-01183-9

Joseph, L., Skliris, N., Dey, D., Marsh, R., & Hirschi, J. (2024). Increased summer monsoon rainfall over northwest India caused by Hadley cell expansion and Indian Ocean warming. *Geophysical Research Letters*, *51*(16), e2024GL108829. https://doi.org/10.1029/2024gl108829

Kajakokulan, P., Pathirana, G., Dheerasinghe, M., & Edirisooriya, I. (2023). Influence of Indian Ocean warming on rainfall of Sri Lanka. *International Journal of Climatology*, *43*(11), 4917–4926. https://doi.org/10.1002/joc.8124

Karlowska, E., Matthews, A. J., Webber, B. G. M., Graham, T., & Xavier, P. (2024). The relative importance of ocean advection and surface heat fluxes during the Madden–Julian oscillation in a coupled ocean–atmosphere model. *Journal of Geophysical Research: Oceans*, *129*(11), e2024JC021515. https://doi.org/10.1029/2024JC021515

Li, B., Zhou, L., Qin, J., & Murtugudde, R. (2022). Increase in intraseasonal rainfall driven by the Arabian Sea warming in recent decades. *Geophysical Research Letters*, *49*(20), e2022GL100536. https://doi.org/10.1029/2022gl100536

Mathew, S., Natesan, U., Latha, G., & Venkatesan, R. (2018). Dynamics behind warming of the southeastern Arabian Sea and its interruption based on in situ measurements. *Ocean Dynamics*, *68*(4), 457–467. https://doi.org/10.1007/S10236-018-1130-3

McMonigal, K., Gunn, K. L., Beal, L. M., Elipot, S., & Willis, J. K. (2022). Reduction in meridional heat export contributes to recent Indian Ocean warming. *Journal of Physical Oceanography*, *52*(3), 329–345. https://doi.org/10.1175/JPO-D-21-0085.1

Nisha, P., Pranesha, T., Vidya, P., Ravichandran, M., & Murtugudde, R. (2023). Trend and interannual variability of the Arabian Sea heat content. *Journal of Marine Systems*, *242*, 103935. https://doi.org/10.1016/j.jmarsys.2023.103935

OpenAI. (2024). Chatgpt: Chatbot based on GPT language model [Software]. Retrieved from https://openai.com/chatgpt

Oppo, D. W., & Rosenthal, Y. (2010). The great indo-pacific communicator. *Science*, *328*(5985), 1492–1494. https://doi.org/10.1126/SCIENCE.1187273

Pradhan, P. K., Kumar, V., Mishra, A. K., Pandey, L. K., & Rao Dabbugottu, N. (2025). Decadal variability of tropical cyclone genesis factors over the Arabian Sea during post-monsoon season. *Meteorology*, *4*(2), 8. https://doi.org/10.3390/meteorology4020008

Pratik, K., Parekh, A., Karmakar, A., Chowdary, J. S., & Gnanaseelan, C. (2018). Recent changes in the summer monsoon circulation and their impact on dynamics and thermodynamics of the Arabian Sea. *Theoretical and Applied Climatology*, *136*(1–2), 321–331. https://doi.org/10.1007/s00704-018-2493-6

Quenouille, M. H. (1952). *Associated measurements*. Butterworths Scientific Publications, Academic Press Inc.

Rainville, L., Lee, C. M., Arulananthan, K., Jinadasa, S. U. P., Fernando, H. J. S., Priyadarshani, W. N. C., & Wijesekera, H. (2022). Water mass exchanges between the Bay of Bengal and Arabian Sea from multiyear sampling with autonomous gliders. *Journal of Physical Oceanography*, *52*(10), 2377–2396. https://doi.org/10.1175/JPO-D-21-0279.1

Rajeevan, M., Srinivasan, J., Niranjan Kumar, K., Gnanaseelan, C., & Ali, M. M. (2013). On the epochal variation of intensity of tropical cyclones in the Arabian Sea. *Atmospheric Science Letters*, *14*(4), 249–255. https://doi.org/10.1002/asl2.447

Roberts, C. D., Palmer, M. D., Allan, R. P., Desbruyeres, D., Hyder, P., Liu, C., & Smith, D. (2017). Surface flux and ocean heat transport convergence contributions to seasonal and interannual variations of ocean heat content. *Journal of Geophysical Research: Oceans*, *122*(1), 726–744. https://doi.org/10.1002/2016JC012278

Roxy, M. K., Gnanaseelan, C., Parekh, A., Chowdary, J. S., Singh, S., Modi, A., et al. (2020). Indian Ocean warming. In R. Krishnan, J. Sanjay, C. Gnanaseelan, M. Mujumdar, A. Kulkarni, & S. Chakraborty (Eds.), *Assessment of climate change over the Indian region: A report of the ministry of earth sciences (MOES), government of India* (pp. 191–206). Springer Singapore. https://doi.org/10.1007/978-981-15-4327-2_10

Roxy, M. K., Ritika, K., Terray, P., Murtugudde, R., Ashok, K., & Goswami, B. N. (2015). Drying of Indian subcontinent by rapid Indian Ocean warming and a weakening land-sea thermal gradient. *Nature Communications*, *6*(1), 7423. https://doi.org/10.1038/ncomms8423

Roxy, M. K., Ritika, K., Terray, P., & Masson, S. (2014). The curious case of Indian Ocean warming. *Journal of Climate*, *27*(22), 8501–8509. https://doi.org/10.1175/JCLI-D-14-00471.1

Sanchez-Franks, A., Webber, B. G. M., King, B. A., Vinayachandran, P. N., Matthews, A. J., Sheehan, P. M. F., et al. (2019). The railroad switch effect of seasonally reversing currents on the Bay of Bengal high-salinity core. *Geophysical Research Letters*, *46*(11), 6005–6014. https://doi.org/10.1029/2019GL082208

Sandeep, S., & Ajayamohan, R. S. (2014). Poleward shift in Indian summer monsoon low level jetstream under global warming. *Climate Dynamics*, *45*(1–2), 337–351. https://doi.org/10.1007/s00382-014-2261-y

Schott, F. A., & McCreary, J. P. (2001). The monsoon circulation of the Indian Ocean. *Progress in Oceanography*, *51*(1), 1–123. https://doi.org/10.1016/S0079-6611(01)00083-0

Schott, F. A., Xie, S., & McCreary, J. P. (2009). Indian Ocean circulation and climate variability. *Reviews of Geophysics*, *47*(1), RG1002. https://doi.org/10.1029/2007rg000245

Shee, A., Sil, S., & Gangopadhyay, A. (2023). Recent changes in the upper oceanic water masses over the Indian Ocean using argo data. *Scientific Reports*, *13*(1), 20252. https://doi.org/10.1038/s41598-023-47658-9

Shetye, S., Gouveia, A., & Shenoi, S. (1994). Circulation and water masses of the Arabian sea. *Proceedings of the Indian Academy of Sciences Earth & Planetary Sciences*, *103*(2), 107–123. https://doi.org/10.1007/BF02839532

Skliris, N., Marsh, R., Haigh, I. D., Wood, M., Hirschi, J., Darby, S., et al. (2022). Drivers of rainfall trends in and around mainland southeast Asia. *Frontiers in Climate*, *4*, 926568. https://doi.org/10.3389/fclim.2022.926568

Swanson, K. L., & Tsonis, A. A. (2009). Has the climate recently shifted? *Geophysical Research Letters*, *36*(6), 209. https://doi.org/10.1029/2008GL037022

Swapna, P., Krishnan, R., & Wallace, J. M. (2013). Indian ocean and monsoon coupled interactions in a warming environment. *Climate Dynamics*, *42*(9–10), 2439–2454. https://doi.org/10.1007/s00382-013-1787-8

Varkey, M., Murty, V., & Suryanarayana, A. (1996). Physical oceanography of the Bay of Bengal. In *Oceanography and marine biology an annual review* (Vol. 34).

Yadav, R. K., & Roxy, M. K. (2019). On the relationship between North India summer monsoon rainfall and east equatorial Indian Ocean warming. *Global and Planetary Change*, *179*, 23–32. https://doi.org/10.1016/j.gloplacha.2019.05.001

Zhang, J., Hu, R., Ma, Q., & Niu, M. (2022). The warming of the Arabian Sea induced a northward summer monsoon over the Tibetan Plateau. *Journal of Climate*, *35*(23), 7541–7554. https://doi.org/10.1175/jcli-d-22-0273.1

Zhang, Y., Zhang, Y., Feng, M., Feng, M., Du, Y., Phillips, H. E., & McPhaden, M. J. (2018). Strengthened Indonesian throughflow drives decadal warming in the southern Indian Ocean. *Geophysical Research Letters*, *45*(12), 6167–6175. https://doi.org/10.1029/2018GL078265